Removal of fluoride from water using activated carbon fibres modified with zirconium by a drop-coating method

Tianting Pang[1], Thet Su Aye Chan[1], Yusufu Abeid Chande Jande[2,3], Junjie Shen[1,4,5*]

[1]Department of Chemical Engineering, University of Bath, Bath BA2 7AY, UK

[2]Water Infrastructure and Sustainable Energy Futures (WISE-Futures) Center, Nelson Mandela African Institution of Science and Technology, Arusha, Tanzania

[3]Department of Materials and Energy Science and Engineering, Nelson Mandela African Institution of Science and Technology, Arusha, Tanzania

[4]Centre for Advanced Separations Engineering (CASE), University of Bath, Bath BA2 7AY, UK

[5]Water Innovation and Research Centre (WIRC), University of Bath, Bath BA2 7AY, UK

Resubmitted to

Chemosphere

April 2020

Word count: 5251 words + 4 figures

*Corresponding author: J.Shen@bath.ac.uk

Abstract:

Metal-modified carbon materials have been widely used for fluoride removal, but the traditional impregnation by soaking method suffers from low loading of metals and substantial use of chemicals. This study proposed a new approach to prepare zirconium modified activated carbon fibres (Zr-ACF) by a drop-coating method. Using the same amount of chemicals, the drop-coating method yielded a 5.5 times higher fluoride adsorption capacity than the soaking method due to more effective loading of Zr(IV) onto ACF. The effects of various preparation conditions, including the addition of a complexing agent (oxalic acid) and Zr/ACF mass ratio (0-1), were investigated. Zr-ACF prepared by drop-coating was characterised by SEM and BET, and the functional groups involved in the anchoring of Zr(IV) on ACF and the adsorption of fluoride onto Zr-ACF were identified by FTIR and XPS. Adsorption experiments at pH between 3 and 11 revealed that ion exchange and electrostatic attraction were the main adsorption mechanisms at different pH levels. Co-existing anions such as CO_3^{2-}, HCO_3^- and Cl^- had an insignificant negative impact (<5%) on fluoride adsorption capacity while SO_4^{2-} decreased fluoride adsorption capacity by 11.5%. The adsorption kinetics followed the pseudo-second-order model. The adsorption isotherms followed the Langmuir isotherm model with a maximum fluoride adsorption capacity of 28.50 mg/L at 25 °C, which was higher than other carbon-based materials in the literature. The remarkable improvement of adsorption capacity and reduced chemical consumption demonstrate that Zr-ACF prepared by drop-coating is a promising adsorbent for fluoride removal.

Keywords:

Drop-coating; activated carbon fibre; zirconium; fluoride; adsorption

1. Introduction

Fluorine is abundant in the natural environment and can be accumulated in the human body via food and water (Akuno et al., 2019). A low concentration of fluoride in water (< 1 mg/L) is beneficial for preventing dental caries and tooth decay (Petersen and Ogawa, 2016). Conversely, long-time ingestion of high concentrations of fluoride causes many health problems such as dental and skeletal fluorosis (Ali et al., 2016), lower intelligence of children (Green et al., 2019) and bone cancer (Crnosija et al., 2019). The World Health Organization (WHO) recommends a fluoride guideline value in drinking water of 1.5 mg/L (World Health Organization, 2017). Globally, more than 200 million people suffer from excess fluoride in drinking water, particularly in developing countries such as Kenya (Malago et al., 2017), Tanzania (Fawell et al., 2006), India (Mukherjee and Singh, 2018; Ali et al., 2019), Iran (Amini et al., 2016; Dehghani et al., 2019; Yousefi et al., 2019) and China (Wang et al., 2019; Zhang et al., 2020).

Adsorption is one of the most used methods for defluoridation due to its simple operation, low energy consumption, and low cost, compared with other methods such as ion exchange (Sundaram and Meenakshi, 2009), coagulation (He et al., 2016; Gan et al., 2019), flocculation (Wang et al., 2013), precipitation (Lu and Liu, 2010), reverse osmosis (Shen and Schäfer, 2015; Owusu-Agyeman et al., 2019) and electrodialysis (Grzegorzek and Majewska-Nowak, 2016). Carbon-based adsorbents with high surface area and low-cost precursor sources, including activated carbon (Talat et al., 2018), carbon nanotubes (Ansari et al., 2011), and activated carbon

fibre (ACF) (Bhaumik and Mondal, 2015), have attracted great attention in recent years. But the physical interactions between these carbon adsorbents and fluoride are still weak which restricts their adsorption capacity. Metal oxides and hydroxides have been used to modify carbon adsorbents, which can not only increase surface area but also enhance the interactions with fluoride. Successful examples include lanthanum (La) modified granular activated carbon (GAC) (Vences-Alvarez et al., 2015), zirconium (Zr) modified GAC (Velazquez-Jimenez et al., 2013), Zr modified powdered activated carbon (PAC) (Mullick and Neogi, 2018), aluminium (Al) and cerium (Ce) modified GAC (Kalidindi et al., 2016), and titanium (Ti) modified PAC (Li et al., 2018).

Impregnation by soaking is a well-established method to modify the carbon-based adsorbents. After impregnation by soaking, the specific surface area of adsorbents can increase up to 10 times (García-Sánchez et al., 2016) and their defluoridation capacities also rise (Daifullah et al., 2007; Nie et al., 2012). However, the amount of metal oxides and hydroxides used in the soaking method is far more than what is required, which may lead to the formation of metallic crystals that are unevenly distributed in the pores and cause channel blockage (Velazquez-Jimenez et al., 2013). This is why the adsorption capacity is not proportional to the amount of metal used, especially in a high concentration soaking solution. To solve this problem, researchers proposed to use complexing agents such as oxalic acid, citric acid, and malic acid (Wang et al., 2011; Velazquez-Jimenez et al., 2013) to improve metal dispersion and control the growth of nucleation. But such extra consumption of chemicals results in significant waste and is against the goal of Green Chemistry.

Drop-coating is another impregnation method which applies a thin layer of a solution dropwise to the surface of the sample and allows it to evaporate. To achieve the same level of

impregnation, the drop-coating method consumes much fewer chemicals and water than the soaking method, thus having a lower process mass intensity (PMI) (Welton, 2015). In recent years, this method has been successfully applied in acoustic chemical sensor arrays (Li, 2011) and enhanced Raman spectroscopy (Halvorson et al., 2011).

This research adopted the drop-coating method to modify ACF with Zr. ACF was preferably used over other carbon-based materials because of its larger surface area, more uniform micropore size distribution and fabric form for ease of handling (Saha and Grappe, 2017). Zr was chosen due to its strong and selective affinity towards fluoride (Górski et al., 2005). Various preparation parameters including the addition of complexing agents and Zr/ACF mass ratio were optimized. Zr-ACF was systematically characterised by SEM, BET, FTIR and XPS. The effects of solution pH and co-existing anions on the defluoridation process were researched and the possible fluoride adsorption mechanisms were proposed. Adsorption kinetics, isotherms, and thermodynamics were also studied.

2. Materials and methods

2.1. Materials and chemicals

The commercial knitted ACF, FLEXZORB FM50K, was obtained from Chemviron Carbon Cloth Division, UK. Zirconium(IV) dichloride oxide octahydrate ($ZrOCl_2 \cdot 8H_2O$), oxalic acid (OA), sodium fluoride (NaF), sodium chloride (NaCl), sodium bicarbonate ($NaHCO_3$), sodium carbonate (Na_2CO_3), sodium sulphate (Na_2SO_4), potassium chloride (KCl), sodium hydroxide (NaOH), hydrochloric acid (HCl), and nitric acid (HNO_3) were purchased from Fisher

Scientific, UK. All the chemicals were of analytical grade. Deionized (DI) water was produced by PURELAB Chorus, ELGA, UK.

2.2. Preparation of adsorbents

Pre-treatment. The as-received ACF was cleaned with 5 M HNO_3 and was repeatedly rinsed with DI water until the pH of the washing liquid was close to 7. Afterwards, ACF was dried in an oven at 105 ºC for 12 h before use.

Impregnation. The Zr-ACF adsorbents were prepared by two wet impregnation methods, namely soaking and drop-coating. The soaking method was modified from a previous study which used OA as the complexing agent (Velazquez-Jimenez et al., 2013). Briefly, 0.1 g of ACF was sheared to the desired size fragment (0.4-0.6 cm) and was soaked into 10 mL of Zr(IV) solution (Zr/ACF mass ratio = 1). The Zr-ACF suspension was stirred for 1 h and then was mixed with 10 mL of OA solution (Zr/OA mass ratio = 1.5) and stirred for another 1 h. The solid Zr-ACF was collected by filtration, washed with DI water, and dried at 105 ºC for 12 h. For comparison purposes, Zr-ACF that did not contain OA was prepared by soaking 0.1 g of ACF into 20 mL of Zr(IV) solution (Zr/ACF mass ratio = 1) for 2 h.

The drop-coating method used Zr(IV) solutions with a much smaller volume. Briefly, 0.1 g of ACF was uniformly drop-coated with 2 mL of Zr(IV) solution (Zr/ACF mass ratio = 0.2-1) and was dried in the oven at 105 ºC for 12 h. Subsequently, Zr-ACF was drop-coated with 4 mL of OA solution (Zr/OA mass ratio = 1.5) and was dried again in the oven at 105 ºC for 12 h. For comparison purposes, Zr-ACF that did not contain OA was prepared by drop-coating 0.1 g of ACF with 2 mL of Zr(IV) solution (Zr/ACF mass ratio = 0.2-1). To ensure that the impregnated

Zr(IV) does not leak from Zr-ACF, some Zr-ACF samples were washed with DI water after drying and their adsorption capacities were compared to the unwashed Zr-ACF.

2.3. Characterization techniques

The surface morphology of ACF and Zr-ACF was observed by a scanning electron microscope (SEM) (JSM-6480LV, JEOL, Japan). Nitrogen adsorption-desorption isotherms were performed at 77 K using a 3Flex Surface Characterization Analyzer (Micromeritics, USA). The specific surface area was calculated from the BET theory and the pore size distribution and pore volume were calculated using the Horvath-Kawazoe model. Fourier-transform infrared spectroscopy (FTIR) analysis was conducted using a Frontier FTIR spectrometer (PerkinElmer, USA) with KBr pellets. The FTIR spectra were recorded with 32 scans at a resolution of 4 cm^{-1}. X-ray photoelectron spectroscopy (XPS) measurements were performed by an AXIS Ultra DLD system (Kratos, UK) using monochromatic Al Ka X-ray source operating at 120 W. XPS data were analysed using CasaXPS (v2.3.19 rev 1.1l) after subtraction of a Shirley background. The pH value at the point of zero charge (pH_{PZC}) was determined by the batch equilibration technique (Shen et al., 2018). A solution of 0.1 M KCl was prepared and its initial pH was adjusted between 3 and 11 by using 0.1 M HCl/NaOH solution. 200 mg of Zr-ACF was added to 100 mL of KCl solution and the suspension was stirred at 298 K for 24 h until the pH stabilized. The final pH was measured and the difference between initial and final pH ($pH_{initial}$-pH_{final}) was plotted against the initial pH. The pH_{PZC} was obtained from the intersection point of the plot. The speciation of fluoride in NaF solution was calculated by using Visual MINTEQ version 3.1 (KTH, Sweden).

2.4. Adsorption experiments

The adsorption of fluoride onto Zr-ACF was carried out in batch adsorption experiments. Fluoride stock solution of 200 mg/L was prepared by dissolving 0.221g of NaF in 500 mL of DI water. Other fluoride solutions were made by subsequent dilutions of the stock solution. A fixed Zr-ACF dose of 2 g/L was used in all experiments.

In a typical adsorption experiment, 200 mg of Zr-ACF was added to 100 mL of 20 mg/L fluoride solution and stirred on the hotplate at 400 rpm and 25 ºC. At regular intervals, 5 mL of the suspension was withdrawn and centrifugated by a benchtop centrifuge (Medifuge, Thermo Scientific, UK). The fluoride concentration in the supernatant was determined by a pH/ion meter coupled with a fluoride ion-selective electrode (S220 and perfectION, Mettler Toledo, USA). Before measurement, the sample was mixed with an equal volume of the total ionic strength adjustment buffer (TISAB II) solution to minimize the effects of complexions and solution pH. The adsorption capacity of Zr-ACF (q_t, mg/g) was calculated from Equation (1) (Dehghani et al., 2017):

$$q_t = \frac{(C_0 - C_t)V}{m} \quad (1)$$

where C_0 and C_t are the initial and present fluoride concentrations (mg/L), V is the volume of the solution (mL), and m is the mass of the adsorbent used (g).

To investigate the effect of solution pH on adsorption capacity, the initial pH of the fluoride solution was adjusted from 3 to 11 (increment by 2) by using 1 mM HCl or 1 mM NaOH solution. The final pH after fluoride adsorption was also measured. To study the effect of

co-existing anions, solutions containing 20 mg/L of fluoride and 20 mg/L of another anion (chloride, bicarbonate, carbonate, and sulphate) were prepared. The methods and equations to determine the adsorption kinetics, isotherms and thermodynamics were included in the Supplementary Information. All the experiments were done in triplicate and the average values of the results were used for data analysis.

3. Results and discussion

3.1. Optimization of the preparation methods

3.1.1. Different impregnation methods

When comparing the effectiveness of different impregnation methods, only the adsorbents with the same Zr/ACF and Zr/OA mass ratios were used. The fluoride adsorption capacities of Zr-ACF prepared by different impregnation methods are shown in Figure 1(A). It can be seen that the drop-coating method yielded a q_e of 8.69 mg/g without OA, and 7.38 mg/g with OA. These values were 5.5 and 3.7 times higher than those of the soaking method, respectively. Besides, water-washed Zr-ACF and unwashed Zr-ACF showed the same level of fluoride adsorption capacity, which indicates that the impregnated Zr(IV) did not leak into aqueous solutions. Given the fact that both impregnation methods consumed the same amount of chemicals, the superior fluoride adsorption capacity of drop-coating was due to more effective loading of Zr(IV) onto ACF. Specifically, the drop-coating method took advantage of higher Zr(IV) concentrations (because of smaller solution volume) and repeated dropwise impregnations. Therefore, to achieve the same level of defluoridation performance, the drop-

coating method consumes much fewer chemicals and water and has a much lower PMI than the soaking method.

Notably, the addition of OA had opposite effects on fluoride adsorption in the drop-coating and the soaking methods. Zr(IV) species can interact with −OH from OA to form zirconium oxalate complexes. The formation of these complexes reduces the number of available binding sites in Zr(IV) for attracting fluoride. This is why the adsorption capacity of Zr-ACF dropped after OA was added in the drop-coating method. Moreover, the high local concentration of OA could reach a supersaturation level and thus the formed complexes could precipitate and cause pore blockage of Zr-ACF.

In the soaking method, on the contrary, the adsorption capacity of Zr-ACF had a slight increase after OA was added, which is consistent with a previous study (Velazquez-Jimenez et al., 2013). This is because the zirconium oxalate complexes prevented the aggregation of Zr particles in the solution due to steric effects and electrostatic repulsion, thus improving the distribution of Zr on the surface of ACF (Velazquez-Jimenez et al., 2013). Since the soaking method had a very low Zr loading, such improvement outweighed the loss of binding sites.

The results revealed that the drop-coating method without OA was the best impregnation method. In the following experiments, only Zr-ACF prepared by drop-coating without OA was used.

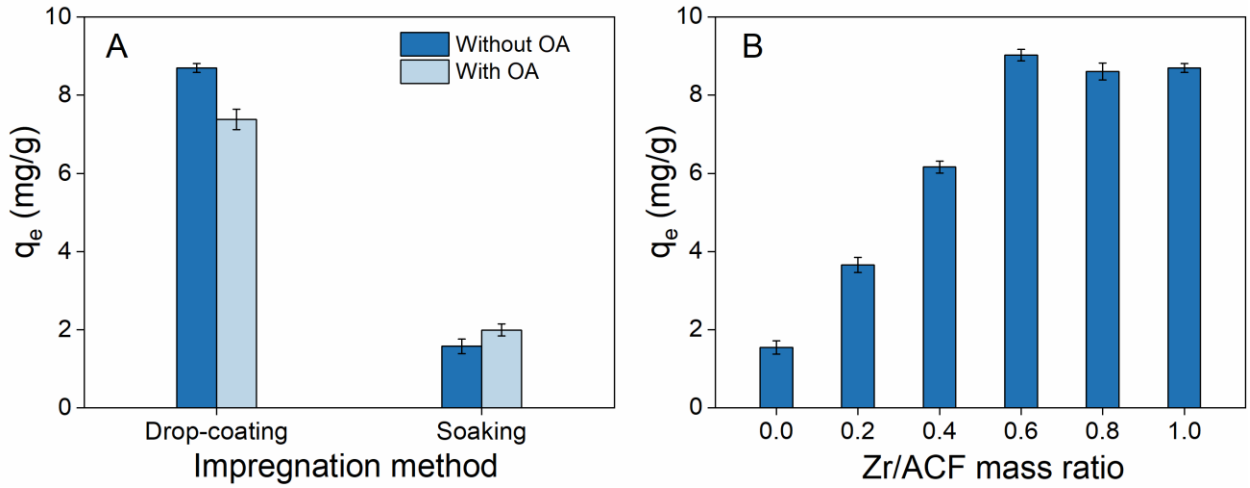

Figure 1: (A) Effect of impregnation method on fluoride adsorption capacity of Zr-ACF and (B) effect of Zr/ACF mass ratio on fluoride adsorption capacity of Zr-ACF (20 mg/L F^-, 2 g/L Zr-ACF, pH 7, 25 ºC)

3.1.2. Different Zr/ACF mass ratios

As shown in Figure 1(B), the adsorption capacity of Zr-ACF increased gradually with the increase of Zr/ACF mass ratio at the beginning and then reached the highest point (9.02 mg/g) when Zr/ACF mass ratio was 0.6, which was 5.8 times higher than that of the original ACF (1.54 mg/g). The amount of Zr(IV) loaded on the surface of ACF surface rose, and thus the binding sites for fluoride increased. As the Zr/ACF mass ratio increased further, the fluoride adsorption capacity declined slightly and remained relatively stable when the Zr/ACF mass ratio reached to 1. The moderate decrease might be because a high concentration of Zr(IV) is unfavourable to form a uniform distribution in the channel of ACF, resulting in channel blockage (Velazquez-Jimenez et al., 2013). Although the adsorption capacity of Zr-ACF at the Zr/ACF mass ratio of 1 (8.69 mg/g) was slightly higher than that at the mass ratio of 0.8 (8.61 mg/g), such minor improvement might be because the detached Zr(IV) species reacts with fluoride and forms

complexes in solution. Considering the trade-off between adsorption capacity and chemical consumption, a moderate Zr/ACF mass ratio of 0.6 was chosen as the fixed mass ratio for further study.

3.2. Characterization of Zr-ACF prepared by drop-coating

3.2.1. Morphology

The surface morphology of original ACF, Zr-ACF before and after fluoride adsorption was analysed using SEM as shown in Figure S1. It can be seen that the porous surface of ACF was uneven and rough which is due to the large pores of ACF. There were grooves and gaps between long carbon fibres. After ACF was modified by Zr, its surface became smooth and the porous structure disappeared, which is because the large pores of ACF were loaded with Zr. After Zr-ACF was saturated by fluoride, the surface of Zr-ACF became even smoother, suggesting that the Zr-F complexes might block the channel of Zr-ACF.

3.2.2. Surface area and pore size distribution

The summary of BET surface area and Horvath-Kawazoe pore volume is shown in Table S1. After drop-coating with Zr, the BET surface area of ACF increased moderately from 1108.60 to 1178.96 m^2/g. After adsorption of fluoride, the BET surface area of Zr-ACF decreased dramatically to 768.54 m^2/g. The Horvath-Kawazoe pore volume followed the same trend, which increased from 0.43 to 0.46 cm^3/g after ACF was modified by Zr, and then declined to 0.31 cm^3/g after fluoride adsorption. As shown in Figure S2, the original ACF displayed a monomodal pore size distribution with the peak at 0.6 nm, which indicates that ACF belongs to microporous materials (Rouquerol et al., 1994). When the ACF was modified by Zr, the pore size distribution became bimodal, with a larger peak at about 0.5 nm and a smaller peak at about

0.6 nm. After fluoride adsorption, the pore size distribution was still bimodal but the pore volumes at two peaks were reduced by almost 50%, which suggests that these micropores contribute most to the adsorption capacity of Zr-ACF.

3.3. Spectroscopic evidence for Zr anchoring on ACF and fluoride adsorption onto Zr-ACF

3.3.1. FTIR analysis

FTIR spectra of ACF, Zr-ACF before and after fluoride adsorption were investigated to illustrate the change of surface functional groups (Figure 2). For ACF, the broad peak centred at 3441 cm^{-1} is due to stretching of −OH groups in adsorbed water (Yu et al., 2018). The peak at 1635 cm^{-1} is the stretching of C=O bonds of −COOH groups. The peaks at 2331 and 2350 cm^{-1} are due to the presence of atmospheric CO_2 on the ACF surface.

For Zr-ACF, the broad −OH peak was blue-shifted due to the formation of Zr−OH groups (Bollino et al., 2017). The C=O bonds had a slight shift because Zr(IV) species interacts with −COOH groups through electrostatic interactions to form C−O−Zr bonds (Velazquez-Jimenez et al., 2013). The peak at 1160 cm^{-1} is due to the combined effects of Zr−OH and C−O groups, as the double bond in −COOH group breaks down and forms new bonds with Zr(IV). The peaks at 1060 cm^{-1} may be associated with the vibration of Zr=O bonds (Mullick and Neogi, 2018). The broad peaks between 980 and 845 cm^{-1} represent a combination of Zr−O and Zr−OH bonds (Velazquez-Jimenez, 2014). The peaks between 718 and 660 cm^{-1} are due to the bending of Zr−OH bonds, formed from combining with −OH groups on ACF surface (Yakout and Hassan, 2014). The small peaks at 491 cm^{-1} can also be attributed to Zr−O bonds (Vitanov et al., 2014).

For Zr-ACF after fluoride adsorption, the −OH peak had a lower intensity than that before fluoride adsorption, which indicates that −OH groups played a role in the fluoride adsorption

process. The C=O peak was further shifted to 1670 cm^{-1} due to the interaction between Zr on the C−O−Zr bond and F^-. The broad peaks between 980 and 845 cm^{-1} are of a greater intensity compared to that before fluoride adsorption which may suggest additional absorption by Zr−O bonds in $ZrOF_2$ formations (Gong et al., 2012). Small peaks between 600 and 524 cm^{-1} may be due to stretching of Zr−F bonds (Gong et al., 2012).

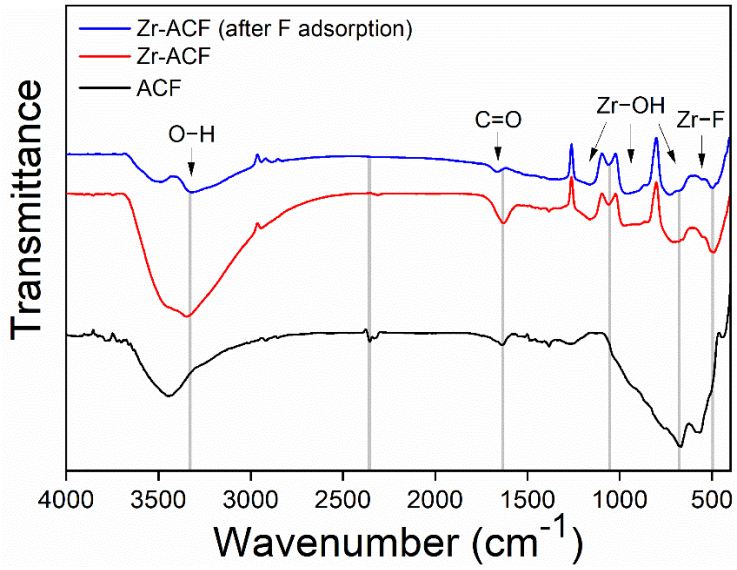

Figure 2: FTIR spectra of original ACF, Zr-ACF before and after fluoride adsorption

3.3.2. XPS analysis

XPS analysis was conducted to seek out the probable Zr(IV) structure formed during the drop-coating process and the way that fluoride interacts with the metal complex. XPS spectra in the C 1s region are demonstrated in Figure 3(A), (B) and (C) representing original ACF, Zr-ACF before and after fluoride adsorption, respectively. For all the three samples, the highest intensity peak is at 284.6 eV, which is attributed to sp^2 C=C bonds. The broad asymmetric tail towards

285 increasing binding energy indicates a high concentration of sp^2 carbon in the samples. All
286 samples showed peaks for C=O and O−C=O bonds at 287.9 eV and 288.9 eV, respectively.
287 From ACF to Zr-ACF, the peak associated with sp^3 carbon bonding was shifted from 286.0
288 to 284.9 eV and was at a higher intensity, suggesting that carbon atoms on the surface of ACF
289 undergo sp^3 hybridisation to form bonds with Zr(IV). Modifying the surface with the less
290 electronegative element Zr increases the electronc density around the base element and decreases
291 the binding energy (Tardio and Cumpson, 2018). After Zr-ACF was saturated by fluoride, the
292 intensity of the O−C=O peak at 288.9 eV declined noticeably. Such change is due to the
293 interaction between Zr on the C−O−Zr bond and F, which was also revealed by the FTIR spectra.
294 Figure 3(D) shows the XPS spectra in the Zr 3d region corrected to C 1s region. The
295 doublet peaks at 182.7 eV and 185.1 eV correspond to Zr−OH bonds in Zr 3d5/2 and Zr 3d3/2
296 regions, respectively (Gondal et al., 2018). Both the peaks were shifted by 0.1 eV towards higher
297 binding energies after fluoride adsorption. The shift indicates the formation of Zr−F bonds
298 because F is the most electronegative element and thus the binding energy of Zr−F is higher than
299 that of Zr−OH bond (Velazquez-Jimenez et al., 2013). The FTIR and XPS analysis identified the
300 main functional groups involved in both the anchoring of Zr(IV) on ACF and the adsorption of
301 fluoride onto Zr-ACF.

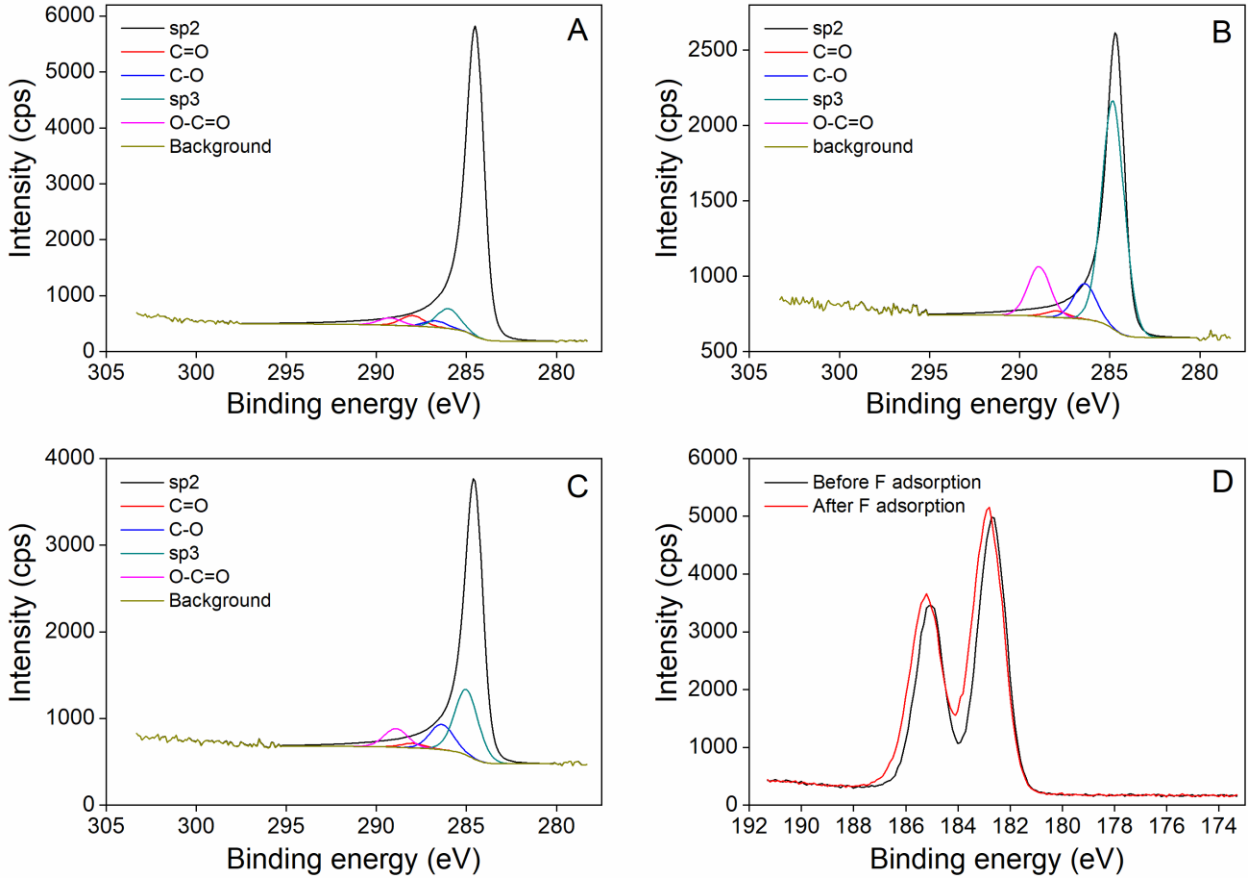

Figure 3: XPS spectra in the C 1s region for (A) ACF, (B) Zr-ACF, (C) Zr-ACF after fluoride adsorption, (D) the Zr 3d region for Zr-ACF before and after fluoride adsorption

3.4. Adsorption mechanisms at different pH levels

The initial pH of the solution plays a critical role in the adsorption process because it changes the surface charge properties of both adsorbent and adsorbate (Sairam Sundaram et al., 2008). As a result, various adsorption mechanisms will occur and affect adsorption behaviours at different pH levels. The surface charge of Zr-ACF was characterized by pH_{PZC} which was found to be 5.6 (Figure S3). The speciation of fluoride was characterized by the acid dissociation constant pKa which is 3.2 (Figure S4). Hence the entire pH range of 3-11 can be distinctly divided into three zones by pH_{PZC} and pKa (Figure 4(A)): in Zone 1 (pH < 3.2), Zr-ACF is

313 positively charged while more than 50% of F species exists as hydrofluoric acid (HF) with no
314 charge; in Zone 2 (3.2 < pH < 5.6), Zr-ACF is still positively charged whereas the majority of F
315 species becomes F^-; in Zone 3 (pH > 5.6), Zr-ACF becomes negatively charged and F^- is also
316 negatively charged.

317 As illustrated in Figure 4(A), q_e increased moderately from Zone 1 to Zone 2 and
318 decreased substantially from Zone 2 to Zone 3. For the experiment in Zone 1, the solution pH
319 increased after fluoride adsorption (Table S2), indicating that fluoride adsorption onto Zr-ACF is
320 primarily the result of ion exchange between F^- and OH^-. As discussed in Section 3.3, the
321 surfaces of Zr-ACF are covered with −OH groups. In the ion exchange process, these −OH
322 groups are replaced by F^-, and new Zr−F covalent bonds are formed between Zr(IV) species
323 (Lewis acid) and F^- (Lewis base) (Wu et al., 2020). The electrostatic attraction between Zr-ACF
324 and partially dissociated F^- may also account for the adsorption.

325 For the experiment in Zone 2, the pH had a smaller increase after fluoride adsorption
326 (Table S2), which means ion exchange still contributes to the adsorption process but to a lesser
327 extent. Instead, the strong electrostatic attraction between Zr-ACF and fully dissociated F^-
328 becomes the principal adsorption mechanism. The maximum q_e of 9.85 mg/g was observed at
329 pH 5 because pH 5 was the nearest to the pH_{PZC} of 5.6.

330 For the experiments in Zone 3, the final pH values were always lower than the initial
331 values (Table S2). This indicates that excessive OH^- in the solution competes with F^- for binding
332 sites on Zr-ACF, which is not beneficial for the ion exchange process. Furthermore, electrostatic
333 forces between Zr-ACF and F^- change from electrostatic attraction to electrostatic repulsion.
334 Therefore, q_e decreased dramatically from Zone 2 to Zone 3.

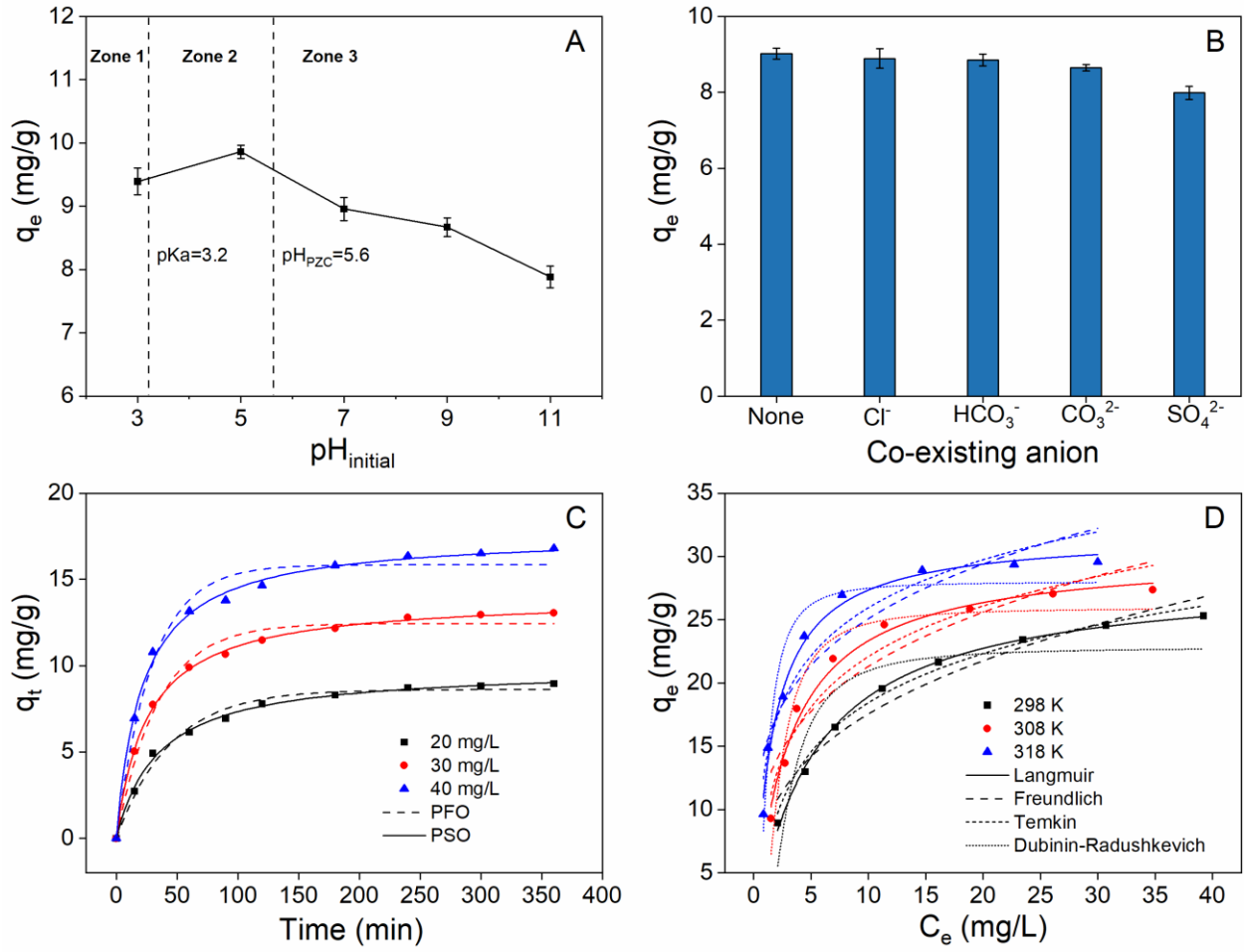

Figure 4: (A) Effect of initial pH on the adsorption capacity of Zr-ACF (20 mg/L F^-, 2 g/L Zr-ACF, 25 ºC); (B) effect of co-existing anions on fluoride adsorption capacity (20 mg/L F^-, 2 g/L Zr-ACF, pH 7, 25 ºC); (C) adsorption kinetics of fluoride onto Zr-ACF at different fluoride concentrations (2 g/L Zr-ACF, pH 7, 25 ºC); (D) adsorption isotherms of fluoride onto Zr-ACF at different temperatures (2 g/L Zr-ACF, pH 7)

3.5. Effect of co-existing anions

Natural waters contain various anions which may interfere with the fluoride adsorption process. As shown in Figure 4(B), the uptake of fluoride by Zr-ACF was affected by co-existing anions in the following order: SO_4^{2-} > CO_3^{2-} > HCO_3^- > Cl^-. Three anions (Cl^-, HCO_3^- and

CO_3^{2-}) had an insignificant negative impact on q_e, which decreased by 1.5%, 1.9% and 4.2%, respectively. It should be noted that some researchers reported that HCO_3^- inhibited the adsorption of fluoride because it had a buffering effect on the solution pH (Kumar et al., 2009; Shen et al., 2018).

By contrast, q_e decreased by 11.5% in the presence of SO_4^{2-}. This is perhaps because SO_4^{2-} has more negative charges and is a stronger Lewis base than F^- (Daifullah et al., 2007); so it can be more strongly attracted to Lewis acid sites on Zr-ACF surface. Moreover, F^- and SO_4^{2-} tend to form inner-sphere complexes with binding surfaces, while other anions such as Cl^- and CO_3^{2-} generally form outer-sphere complexes (Kumar et al., 2011; Wu et al., 2020). Inner-sphere complexation involves a much stronger interaction than outer-sphere complexation. This provides a strong driving force to adsorb F^- from other anions except for SO_4^{2-}.

3.6. Adsorption kinetics, isotherms, and thermodynamics

Adsorption kinetics identify the required equilibrium time for an adsorption process (Tran et al., 2017). As shown in Figure 4(C), fluoride adsorption by Zr-ACF was most rapid in the first 30 minutes with more than 50% of the initial fluoride concentration were removed. Such rapid adsorption rate is due to the initial steep concentration gradient between the solution and the surface of Zr-ACF as well as the large number of vacant pores (Zhang et al., 2018). The adsorption rate then decreased gradually until the equilibrium was reached after 360 min. The kinetics data were fitted to the pseudo-first-order (PFO) and the pseudo-second-order (PSO) models (Figure 4(C)). The equations of the models are provided in the Supplementary Information. The kinetic parameters, together with the standard deviation SD and the coefficient of determination R^2, are listed in Table S3. It can be seen that the PSO model had a higher R^2

(>0.995) and a lower SD than the PFO model under all three fluoride concentrations. Therefore, the PSO model is more suitable for the description of the adsorption kinetics of fluoride onto Zr-ACF. These results are consistent with the adsorption of fluoride onto other adsorbents, such as activated carbon and aluminium hydroxide (Gai et al., 2015; Mullick and Neogi, 2018).

Adsorption isotherms describe the equilibrium relationship between the adsorbate and the adsorbent (Tran et al., 2017; Dehghani et al., 2018). As shown in Figure 4(D), the adsorption capacity of Zr-ACF at equilibrium increased with the increasing temperature, which indicates the endothermic nature of the adsorption process. The experimental data were fitted to four widely used isotherm models, namely the Langmuir, Freundlich, Temkin and Dubinin-Radushkevich (D-R) models. The descriptions of the four models, including their nonlinear equations, are included in the Supplementary Information. The fitting curves of the four models are shown in Figure 4(D) and the isotherms parameters and the coefficient of determination R^2 are given in Table S4. Among the four models, the Langmuir model was found to be best fitted to the experimental data as the R^2 values of the Langmuir model (varied from 0.985 to 0.997) are invariably higher than those of other models at every temperature. This suggests that the fluoride adsorption process is monolayer molecular adsorption and it occurs homogeneously on the surface of Zr-ACF (Langmuir, 1918). The separation factor (R_L) of the Langmuir model, which indicates the favourability of the adsorption process, was calculated and shown in Figure S5. The value of R_L can be either irreversible ($R_L = 0$), favourable ($0 < R_L < 1$), linear ($R_L = 1$), or unfavourable ($R_L > 1$) (Weber and Chakravorti, 1974). The R_L values at all three temperatures were always below 0.25, indicating that the adsorption process was extremely favourable.

Table S5 compares the Langmuir maximum adsorption capacity (q_m) of various carbon-based adsorbents for fluoride removal. The q_m of Zr-ACF prepared in this study was 28.50 mg/g

when the adsorbent dose was 2 g/L, the pH was 7 and the temperature was 25 °C. Apparently, Zr-ACF exhibits superior performance over other carbon-based adsorbents reported in the literature.

Adsorption thermodynamics indicate the feasibility of the adsorption processes. The values of the thermodynamic parameters are shown in Table S6. The negative values of $\Delta G°$ at all three temperatures denote the spontaneity of the adsorption process (Li et al., 2005; Khan et al., 2020). As the temperature rose, the absolute value of $\Delta G°$ increased implying that the adsorption process is more favourable at a higher temperature. The positive values of $\Delta H°$ confirm that the adsorption process is endothermic (Gao et al., 2013). The positive values of $\Delta S°$ imply increasing randomness of the process (Ghaedi et al., 2012). In summary, the adsorption process of fluoride onto Zr-ACF is spontaneous and endothermic.

4. Conclusion

In this study, we have presented a new drop-coating method to prepare Zr-ACF adsorbents for fluoride removal. Compared to the traditional soaking method, the drop-coating method achieved a 5.5 times higher fluoride adsorption capacity while consumed much fewer chemicals and no complexing agents. The optimal Zr/ACF mass ratio for fluoride removal was 0.6. SEM and BET results showed that Zr-ACF prepared by drop-coating had smoother surface and greater surface area than the original ACF. The micropores contribute most to the adsorption capacity of Zr-ACF. FTIR and XPS results showed that −OH groups played a key role in the anchoring of Zr(IV) on ACF and the adsorption of fluoride onto Zr-ACF. Ion exchange and electrostatic attraction were the two main adsorption mechanisms and they dominated in

different pH zones that were divided by pH_{PZC} of Zr-ACF and pKa of fluoride. Various co-existing anions, except for SO_4^{2-}, had insignificant influence on the fluoride adsorption capacity of Zr-ACF. The PSO model was suitable in describing the adsorption kinetics and the Langmuir model was best fit to the isotherms data with the maximum adsorption capacity obtained at 25 °C up to 28.50 mg/L. The thermodynamic study revealed that the adsorption process was spontaneous and endothermic in nature.

The results have demonstrated that Zr-ACF produced by drop-coating is an efficient and cost-effective adsorbent for fluoride removal due to its ease of synthesis, reduced chemical consumption and improved adsorption capacity. The drop-coating method can be easily scaled up by using commercial sprayers, which makes it highly practical in rural and remote areas of developing countries. However, further research is needed to assess the environmental impact of Zr-ACF and develop an appropriate recycling strategy before it can be used for large-scale applications.

Acknowledgements

This research was supported by the Royal Academy of Engineering under the Research Fellowship scheme (RF_201718_17145). XPS data collection was performed at the EPSRC National Facility for XPS (‘HarwellXPS’), operated by Cardiff University and UCL, under contract No. PR16195.

References

Akuno, M.H., Nocella, G., Milia, E.P., Gutierrez, L., 2019. Factors influencing the relationship between fluoride in drinking water and dental fluorosis: a ten-year systematic review and meta-analysis. Journal of Water and Health.

Ali, S., Fakhri, Y., Golbini, M., Thakur, S.K., Alinejad, A., Parseh, I., Shekhar, S., Bhattacharya, P., 2019. Concentration of fluoride in groundwater of India: A systematic review, meta-analysis and risk assessment. Groundwater for Sustainable Development, 100224.

Ali, S., Thakur, S.K., Sarkar, A., Shekhar, S., 2016. Worldwide contamination of water by fluoride. Environmental Chemistry Letters 14, 291-315.

Amini, H., Haghighat, G.A., Yunesian, M., Nabizadeh, R., Mahvi, A.H., Dehghani, M.H., Davani, R., Aminian, A.-R., Shamsipour, M., Hassanzadeh, N., 2016. Spatial and temporal variability of fluoride concentrations in groundwater resources of Larestan and Gerash regions in Iran from 2003 to 2010. Environmental Geochemistry and Health 38, 25-37.

Ansari, M., Kazemipour, M., Dehghani, M., Kazemipour, M., 2011. The defluoridation of drinking water using multi-walled carbon nanotubes. Journal of Fluorine Chemistry 132, 516-520.

Bhaumik, R., Mondal, N.K., 2015. Adsorption of fluoride from aqueous solution by a new low-cost adsorbent: thermally and chemically activated coconut fibre dust. Clean Technologies and Environmental Policy 17, 2157-2172.

Bollino, F., Armenia, E., Tranquillo, E., 2017. Zirconia/hydroxyapatite composites synthesized via Sol-Gel: Influence of hydroxyapatite content and heating on their biological properties. Materials 10, 757.

Crnosija, N., Choi, M., Meliker, J.R., 2019. Fluoridation and county-level secondary bone cancer among cancer patients 18 years or older in New York State. Environmental Geochemistry and Health 41, 761-768.

Daifullah, A., Yakout, S., Elreefy, S., 2007. Adsorption of fluoride in aqueous solutions using KMnO4-modified activated carbon derived from steam pyrolysis of rice straw. Journal of Hazardous materials 147, 633-643.

Dehghani, M.H., Faraji, M., Mohammadi, A., Kamani, H., 2017. Optimization of fluoride adsorption onto natural and modified pumice using response surface methodology: isotherm, kinetic and thermodynamic studies. Korean Journal of Chemical Engineering 34, 454-462.

Dehghani, M.H., Zarei, A., Mesdaghinia, A., Nabizadeh, R., Alimohammadi, M., Afsharnia, M., McKay, G., 2018. Production and application of a treated bentonite–chitosan composite for the efficient removal of humic acid from aqueous solution. Chemical Engineering Research and Design 140, 102-115.

Dehghani, M.H., Zarei, A., Yousefi, M., Asghari, F.B., Haghighat, G.A., 2019. Fluoride contamination in groundwater resources in the southern Iran and its related human health risks. Desalination and Water Treatment 153, 95-104.

Fawell, J., Bailey, K., Chilton, J., Dahi, E., Magara, Y., 2006. Fluoride in drinking-water. IWA publishing.

Gai, W.-Z., Deng, Z.-Y., Shi, Y., 2015. Fluoride removal from water using high-activity aluminum hydroxide prepared by the ultrasonic method. RSC Advances 5, 84223-84231.

Gan, Y., Wang, X., Zhang, L., Wu, B., Zhang, G., Zhang, S., 2019. Coagulation removal of fluoride by zirconium tetrachloride: Performance evaluation and mechanism analysis. Chemosphere 218, 860-868.

Gao, H., Kan, T., Zhao, S., Qian, Y., Cheng, X., Wu, W., Wang, X., Zheng, L., 2013. Removal of anionic azo dyes from aqueous solution by functional ionic liquid cross-linked polymer. Journal of Hazardous materials 261, 83-90.

García-Sánchez, J., Solache-Ríos, M., Martínez-Gutiérrez, J., Arteaga-Larios, N., Ojeda-Escamilla, M., Rodríguez-Torres, I., 2016. Modified natural magnetite with Al and La ions for the adsorption of fluoride ions from aqueous solutions. Journal of Fluorine Chemistry 186, 115-124.

Ghaedi, M., Sadeghian, B., Pebdani, A.A., Sahraei, R., Daneshfar, A., Duran, C., 2012. Kinetics, thermodynamics and equilibrium evaluation of direct yellow 12 removal by adsorption onto silver nanoparticles loaded activated carbon. Chemical Engineering Journal 187, 133-141.

Gondal, M.A., Fasasi, T.A., Baig, U., Mekki, A., 2018. Effects of oxidizing media on the composition, morphology and optical properties of colloidal zirconium oxide nanoparticles synthesized via pulsed laser ablation in liquid technique. Journal of Nanoscience and Nanotechnology 18, 4030-4039.

Gong, Y., Andrews, L., Bauschlicher, C.W., Thanthiriwatte, K.S., Dixon, D., 2012. Infrared spectroscopic and theoretical studies of the OTiF2, OZrF2 and OHfF2 molecules with terminal oxo ligands. Dalton Trans. 41, 11706-11715.

Górski, Ł., Saniewska, A., Parzuchowski, P., Meyerhoff, M.E., Malinowska, E., 2005. Zirconium(IV)-salophens as fluoride-selective ionophores in polymeric membrane electrodes. Analytica Chimica Acta 551, 37-44.

Green, R., Lanphear, B., Hornung, R., Flora, D., Martinez-Mier, E.A., Neufeld, R., Ayotte, P., Muckle, G., Till, C., 2019. Association between maternal fluoride exposure during pregnancy and IQ scores in offspring in Canada. JAMA Pediatrics 173, 940-948.

Grzegorzek, M., Majewska-Nowak, K., 2016. Use of the electrodialysis process for fluoride ion and salt removal from multi-constituent aqueous solutions. Architecture Civil Engineering Environment 9, 107--113.

Halvorson, R.A., Leng, W., Vikesland, P.J., 2011. Differentiation of microcystin, nodularin, and their component amino acids by drop-coating deposition Raman spectroscopy. Analytical Chemistry 83, 9273-9280.

He, Z., Lan, H., Gong, W., Liu, R., Gao, Y., Liu, H., Qu, J., 2016. Coagulation behaviors of aluminum salts towards fluoride: significance of aluminum speciation and transformation. Separation and Purification Technology 165, 137-144.

Kalidindi, S., Vecha, M., Kar, A., Raychoudhury, T., 2016. Aluminum–cerium double-metal impregnated activated carbon: a novel composite for fluoride removal from aqueous solution. Water Supply 17, 115-124.

Khan, Z.H., Gao, M., Qiu, W., Islam, M.S., Song, Z., 2020. Mechanisms for cadmium adsorption by magnetic biochar composites in an aqueous solution. Chemosphere 246, 125701.

Kumar, E., Bhatnagar, A., Ji, M., Jung, W., Lee, S.-H., Kim, S.-J., Lee, G., Song, H., Choi, J.-Y., Yang, J.-S., Jeon, B.-H., 2009. Defluoridation from aqueous solutions by granular ferric hydroxide (GFH). Water Research 43, 490-498.

Kumar, E., Bhatnagar, A., Kumar, U., Sillanpää, M., 2011. Defluoridation from aqueous solutions by nano-alumina: Characterization and sorption studies. Journal of Hazardous materials 186, 1042-1049.

Langmuir, I., 1918. The adsorption of gases on plane surfaces of glass, mica and platinum. Journal of the American Chemical Society 40, 1361-1403.

Li, Y.-H., Di, Z., Ding, J., Wu, D., Luan, Z., Zhu, Y., 2005. Adsorption thermodynamic, kinetic and desorption studies of Pb2+ on carbon nanotubes. Water Research 39, 605-609.

Li, Y., 2011. Surface modification technique for acoustic chemical sensor arrays based on CMUTs.

Li, Y., Zhang, C., Jiang, Y., Wang, T.-J., 2018. Electrically enhanced adsorption and green regeneration for fluoride removal using Ti(OH)4-loaded activated carbon electrodes. Chemosphere 200, 554-560.

Lu, N.C., Liu, J., 2010. Removal of phosphate and fluoride from wastewater by a hybrid precipitation–microfiltration process. Separation and Purification Technology 74, 329-335.

Malago, J., Makoba, E., Muzuka, A.N., 2017. Fluoride levels in surface and groundwater in Africa: A review. American Journal of Water Science and Engineering 3, 1-17.

Mukherjee, I., Singh, U.K., 2018. Groundwater fluoride contamination, probable release, and containment mechanisms: a review on Indian context. Environmental Geochemistry and Health 40, 2259-2301.

Mullick, A., Neogi, S., 2018. Acoustic cavitation induced synthesis of zirconium impregnated activated carbon for effective fluoride scavenging from water by adsorption. Ultrasonics Sonochemistry 45, 65-77.

Nie, Y., Hu, C., Kong, C., 2012. Enhanced fluoride adsorption using Al (III) modified calcium hydroxyapatite. Journal of Hazardous materials 233, 194-199.

Owusu-Agyeman, I., Reinwald, M., Jeihanipour, A., Schäfer, A.I., 2019. Removal of fluoride and natural organic matter from natural tropical brackish waters by nanofiltration/reverse osmosis with varying water chemistry. Chemosphere 217, 47-58.

Petersen, P.E., Ogawa, H., 2016. Prevention of dental caries through the use of fluoride–the WHO approach. Community Dent Health 33, 66-68.

Rouquerol, J., Avnir, D., Fairbridge, C.W., Everett, D.H., Haynes, J.M., Pernicone, N., Ramsay, J.D.F., Sing, K.S.W., Unger, K.K., 1994. Recommendations for the characterization of porous solids (Technical Report). Pure and Applied Chemistry 66, 1739-1758.

Saha, D., Grappe, H.A., 2017. 5 - Adsorption properties of activated carbon fibers. in: Chen, J.Y. (Ed.). Activated Carbon Fiber and Textiles. Woodhead Publishing, Oxford, pp. 143-165.

Sairam Sundaram, C., Viswanathan, N., Meenakshi, S., 2008. Defluoridation chemistry of synthetic hydroxyapatite at nano scale: Equilibrium and kinetic studies. Journal of Hazardous materials 155, 206-215.

Shen, J., Evangelista, M.F., Mkongo, G., Wen, H., Langford, R., Rosair, G., McCoustra, M.R.S., Arrighi, V., 2018. Efficient defluoridation of water by Monetite nanorods. Adsorption 24, 135-145.

Shen, J., Schäfer, A.I., 2015. Factors affecting fluoride and natural organic matter (NOM) removal from natural waters in Tanzania by nanofiltration/reverse osmosis. Science of the Total Environment 527–528, 520-529.

Sundaram, C.S., Meenakshi, S., 2009. Fluoride sorption using organic–inorganic hybrid type ion exchangers. Journal of Colloid and Interface Science 333, 58-62.

Talat, M., Mohan, S., Dixit, V., Singh, D.K., Hasan, S.H., Srivastava, O.N., 2018. Effective removal of fluoride from water by coconut husk activated carbon in fixed bed column: Experimental and breakthrough curves analysis. Groundwater for Sustainable Development 7, 48-55.

Tardio, S., Cumpson, P.J., 2018. Practical estimation of XPS binding energies using widely available quantum chemistry software. Surface and Interface Analysis 50, 5-12.

Tran, H.N., You, S.-J., Hosseini-Bandegharaei, A., Chao, H.-P., 2017. Mistakes and inconsistencies regarding adsorption of contaminants from aqueous solutions: A critical review. Water Research 120, 88-116.

Velazquez-Jimenez, L.H., 2014. Zirconium–Carbon Hybrid Sorbent for Removal of Fluoride from Water: Oxalic Acid Mediated Zr(IV) Assembly and Adsorption Mechanism. Environmental Science & Technology 48, 1166-1175.

572 Velazquez-Jimenez, L.H., Hurt, R.H., Matos, J., Rangel-Mendez, J.R., 2013. Zirconium–carbon
573 hybrid sorbent for removal of fluoride from water: oxalic acid mediated Zr (IV) assembly and
574 adsorption mechanism. Environmental Science & Technology 48, 1166-1174.

575 Vences-Alvarez, E., Velazquez-Jimenez, L.H., Chazaro-Ruiz, L.F., Diaz-Flores, P.E., Rangel-
576 Mendez, J.R., 2015. Fluoride removal in water by a hybrid adsorbent lanthanum–carbon. Journal
577 of Colloid and Interface Science 455, 194-202.

578 Vitanov, P., Harizanova, A., Ivanova, T., 2014. Characterization of ZrO_2 and $(ZrO2)_X(Al2O3)_{1-X}$
579 thin films on Si substrates: effect of the Al_2O_3 component. Journal of Physics: Conference Series
580 514, 012011.

581 Wang, B.-y., Chen, Z.-l., Zhu, J., Shen, J.-m., Han, Y., 2013. Pilot-scale fluoride-containing
582 wastewater treatment by the ballasted flocculation process. Water Science and Technology 68,
583 134-143.

584 Wang, M., Li, X., He, W.-y., Li, J.-x., Zhu, Y.-y., Liao, Y.-L., Yang, J.-y., Yang, X.-e., 2019.
585 Distribution, health risk assessment, and anthropogenic sources of fluoride in farmland soils in
586 phosphate industrial area, southwest China. Environmental Pollution 249, 423-433.

587 Wang, Y., Chen, N., Wei, W., Cui, J., Wei, Z., 2011. Enhanced adsorption of fluoride from
588 aqueous solution onto nanosized hydroxyapatite by low-molecular-weight organic acids.
589 Desalination 276, 161-168.

590 Weber, T.W., Chakravorti, R.K., 1974. Pore and solid diffusion models for fixed-bed adsorbers.
591 AIChE Journal 20, 228-238.

592 Welton, T., 2015. Solvents and sustainable chemistry. Proceedings of the Royal Society A:
593 Mathematical, Physical and Engineering Sciences 471, 20150502.

594 World Health Organization, 2017. Guidelines for drinking-water quality, 4th edition,
595 incorporating the 1st addendum. Switzerland.

596 Wu, B., Wan, J., Zhang, Y., Pan, B., Lo, I.M.C., 2020. Selective phosphate removal from water
597 and wastewater using sorption: Process fundamentals and removal mechanisms. Environmental
598 Science & Technology 54, 50-66.

599 Yakout, S.M., Hassan, H.S., 2014. Adsorption characteristics of sol gel-derived zirconia for
600 cesium ions from aqueous solutions. Molecules (Basel, Switzerland) 19, 9160.

601 Yousefi, M., Ghalehaskar, S., Asghari, F.B., Ghaderpoury, A., Dehghani, M.H., Ghaderpoori, M.,
602 Mohammadi, A.A., 2019. Distribution of fluoride contamination in drinking water resources and
603 health risk assessment using geographic information system, northwest Iran. Regulatory
604 Toxicology and Pharmacology 107, 104408.

Yu, Z., Xu, C., Yuan, K., Gan, X., Feng, C., Wang, X., Zhu, L., Zhang, G., Xu, D., 2018. Characterization and adsorption mechanism of ZrO2 mesoporous fibers for health-hazardous fluoride removal. Journal of Hazardous materials 346, 82-92.

Zhang, L., Zhao, L., Zeng, Q., Fu, G., Feng, B., Lin, X., Liu, Z., Wang, Y., Hou, C., 2020. Spatial distribution of fluoride in drinking water and health risk assessment of children in typical fluorosis areas in north China. Chemosphere 239, 124811.

Zhang, Z., Li, Y., Chen, H., Zhang, X., Li, H., 2018. The systematic adsorption of diclofenac onto waste red bricks functionalized with iron oxides. Water 10, 1343.